# *In vivo* quantitative Magnetization Transfer in the cervical spinal cord using reduced Field-of-View imaging: a feasibility study.

Marco Battiston[1], Francesco Grussu[1], James Fairney[2,3], Ferran Prados[4,1], Sebastien Ourselin[4], Mara Cercignani[5], Claudia AM Gandini Wheeler Kingshott[1,6], Rebecca S Samson[1]

[1] *NMR Research Unit, Queen Square MS Centre, Department of Neuroinflammation, UCL Institute of Neurology, University College London, London, United Kingdom*

[2] *UCL Department of Medical Physics and Biomedical Engineering, University College London, London, England, United Kingdom*

[3] *Department of Brain Repair and Rehabilitation, UCL Institute of Neurology, University College London, London, England, United Kingdom*

[4] *Translational Imaging Group, Centre for Medical Image Computing, UCL Department Medical Physics and Bioengineering, University College London, London, United Kingdom*

[5] *CISC, Brighton & Sussex Medical School, Brighton, Sussex, United Kingdom*

[6] *Brain Connectivity Centre, C. Mondino National Neurological Institute, Pavia, Italy*

**Synopsis:**

Quantitative Magnetization Transfer (qMT) Imaging techniques offer the possibility to estimate tissue macromolecular fraction, which has been shown to be specific for myelin in the brain and spinal cord. To date, applications of qMT in the spinal cord have been hampered by prohibitive protocol duration. We propose a novel approach for qMT in the spinal cord based on the combination of offresonance saturation a small field-of-view imaging, with the potential of reducing scan time needed to perform qMT in the spinal cord.

## Introduction

The spinal cord (SC) is affected in demyelinating diseases of the central nervous system, such as Multiple Sclerosis [1]. Using quantitative Magnetisation Transfer (qMT) methods, it is possible to extract measures related to macromolecular tissue content, which have been shown to be specific for myelin in the brain and SC [2].

However, performing qMT in the SC is challenging, mostly due to the prohibitive scan times required to acquire multiple high resolution images in order to accurately estimate all model parameters. Therefore qMT has not found widespread application *in vivo* in the SC, with just a single study previously published [3]. Efforts have rather aimed on developing simplified versions of the rigorous qMT [4], or optimising semi-quantitative approaches [5,6].

We explored the possibility of performing qMT *in vivo* in the SC within a clinically feasible acquisition time, by combining a train of Magnetization Transfer (MT) off-resonance saturation pulses with a small field-of-view single-shot Echo Planar Imaging (EPI) readout (ZOOM-EPI [7]). The feasibility of the approach is demonstrated in 3 healthy volunteers.

## Materials and Methods

*MRI Acquisition:*

3 healthy volunteers (25-28 years) were imaged using a 3T Philips Achieva scanner with a 32-channel head coil and radio-frequency dual transmit technology.
MT-weighted data were acquired at 18 combinations of frequency offset and MT pulse flip angles, with 6 non-MT-weighted ($M_0$) images interleaved, for an acquisition time of 24mins (details in figure 1). Imaging volume consisted of twelve 5mm-thick axial slices centred at level C2-C3, FOV=51x4mm$^2$, 0.8x0.8mm$^2$ in-plane resolution, TE=27ms, TR=10040ms (4 slices per TR), NSA=2.
A train of off-resonance pulses was applied prior to slice excitation. To avoid contamination between partial saturation in the imaging volume due to the ZOOM-EPI tilted refocus and spatially non-selective MT pulses, a delay of 6.5s was appended after each slice package. Artefact-free images were obtained without outer volume suppression, allowing slice excitation starting immediately after the MT pulse train, thereby almost entirely preserving the MT-weighting.
For $T_1$ estimation, Inversion Recovery (IR) data (6mins) were acquired at 8 different Inversion Times (TI=100, 220, 340, 460, 1300, 1420, 1540, 1660ms) with the same readout as MT-weighted data.

*Data Analysis:*

MT-weighted and IR data were co-registered to the mean of the interleaved $M_0$ images using slice-wise rigid transformations estimated with flirt (http://www.fmrib.ox.ac.uk/fsl/). $M_0$ images were also exploited to characterise the noise distribution, and to normalize MT-weighted signal prior to qMT model fitting.
To account for the slice-dependent MT-weighting and the unmet steady-state condition introduced by the sequence, data were fitted using the Minimal Approximation Magnetization Transfer (MAMT) model [7], implemented in Matlab (The MathWorks Inc., Natick, MA, 2000) using a discretizing step of 120μs. Four model parameters were estimated: the bound pool fraction (BPF),

free water pool transverse relaxation time ($T_2^F$), bound water pool transverse relaxation time ($T_2^B$) and the forward MT exchange rate ($RM_0^B$). A super-Lorentzian lineshape was assumed to describe the bound pool saturation rate. The free water pool longitudinal relaxation rate ($R_1^F$) was obtained via mono-exponential model fitting of IR data, assuming a bound water pool longitudinal relaxation rate ($R_1^B$) of $1s^{-1}$ [9]. Maximum likelihood estimation based on Rician noise was used.

**Results**

Figure 2 shows single slice examples of IR and MT-weighted images used to estimate model parameters. Figure 3 gives single voxel examples of model fitting for the IR and MT experiments. Single slice BPF, $T_2^F$, $T_2^B$, $RM_0^B$ and $T_1$ maps are shown in figure 4 together with the averaged $M_0$ image.

Whole cord parameters median values and interquartile ranges are reported in figure 5. Global mean and standard deviations (SD) were: BPF=10.5(±0.18)%, $T_2^F$=47.5(±3.8)ms, $T_2^B$=10.1(±0.27)μs, $RM_0^B$=1.73(±0.09) and $T_1^{obs}$=1130(36.3)ms.

**Discussion and Conclusions**

Median values reported in figure 5 are consistent with previous findings in brain studies [10], suggesting estimation of two-pool qMT model parameters is feasible with this approach. Visual inspection of parametric maps and parameter values in figure 4 show whole cord distributions for $T_2^F$ and $RM_0^B$ are broader compared to BPF and $T_2^B$, confirming previous findings using the same model in the brain [8, 10], and outcomes of protocol optimisation [11].

In future work a separate acquisition could be used to better estimate $T_2^F$, as in [3], and $B_1$ and $B_0$ corrections should also be implemented.

This novel approach for *in vivo* qMT in the SC using rapid single-shot ZOOM-EPI readout immediately following a train of MT pulses gives improved protocol flexibility, since the MT saturation and image acquisition can be separately designed. The requirement for high resolution data therefore does not interfere with the amount of MT-weighting, which can be optimally designed to achieve time efficiency.

**Acknowledgements**

The UK MS Society and the UCL-UCLH Biomedical Research Centre for ongoing support. UCL Grand Challenges Studentship scheme. Project grants EPSRC EP/I027084/1 and ISRT IMG006; MRC(MR/J500422/1); NIHR BRC UCLH/UCL High Impact Initiative, project grants EPSRC (EP/H046410/1,EP/J020990/1,EP/K005278) and MRC (MR/J01107X/1).

**References**

1-Gilmore CP et al, Mult Scler 15: 180-188 (2009)

2- Ou X et al, Quantitative Magnetization Transfer Measured Pool-Size-Ratio reflects optic nerve myelin content in ex-vivo mice. MRM 61:364-371 (2009).
3- Smith S et al, Quantitative Magnetization Transfer Characteristics of the human cervical spinal cord in vivo: application to adrenomyelonuropathy. MRM 61:22-27 (2009)
4 – Smith A et al. Rapid high-resolution quantitative magnetization transfer MRI of the human spinal cord. NeuroImage (2014)
5 – Samson S R et al, Tissue- and column-specific measurements from multi-parameter mapping of the human cervical spinal cord at 3T. NMR Biomed (2013)
6 – Feasibility of grey matter and white matter segmentation of the upper cervical cord in vivo: a pilot study with application to magnetisation transfer measurements.
7 - Wheeler-Kingshott C AM et al, Investigating cervical spinal cord structure using axial diffusion tensor imaging. Neuroimage 16, 93-102 (2002)
8 – Portnoy S et al, Modeling pulsed magnetization transfer. MRM 58: 144-155 (2007)
9- Henkelman M et al, Quantitative interpretation of Magnetization Transfer. MRM 29:759-766 (1993)
10- Muller et al, Matrix-algebra-based calculations of the time evolution of the binary spin-bath model for magnetization transfer. JMR 230 (2013) 88-97
11 – Cercignani M et al, Optimal acquisition schemes for in vivo quantitative magnetization transfer MRI. MRM 58:803-810 (2006).

| *Parameter* | *Value* |
|---|---|
| $\theta$ [°] | 760, 950, 1500 |
| $\Delta$ [kHz] | 0.8, 1.2, 1.5, 2.2, 5, 10 |
| pulse duration [ms] | 40 |
| pulse gap [ms] | 1 |
| pulse shape | sinc–Gaussian |
| $N_{pulse}$ | 12 |
| $\Delta t_{slice}$ [ms] | 518 |
| $T_{rec}$ [ms] | 6500 |
| TR [ms] | 10040 |

Fgure 1. Resume of sequence parameters of MT-weighted data acquisition: θ (MT pulse flip angle), Δ (MT pulse frequency offset), pulse duration, pulse gap, pulse shape, $N_{pulse}$ (number of pulses per train), $\Delta t_{slice}$ (time interval between MT pulse trains in the same package), $T_{rec}$ (*dead-time* between slice packages), and TR.

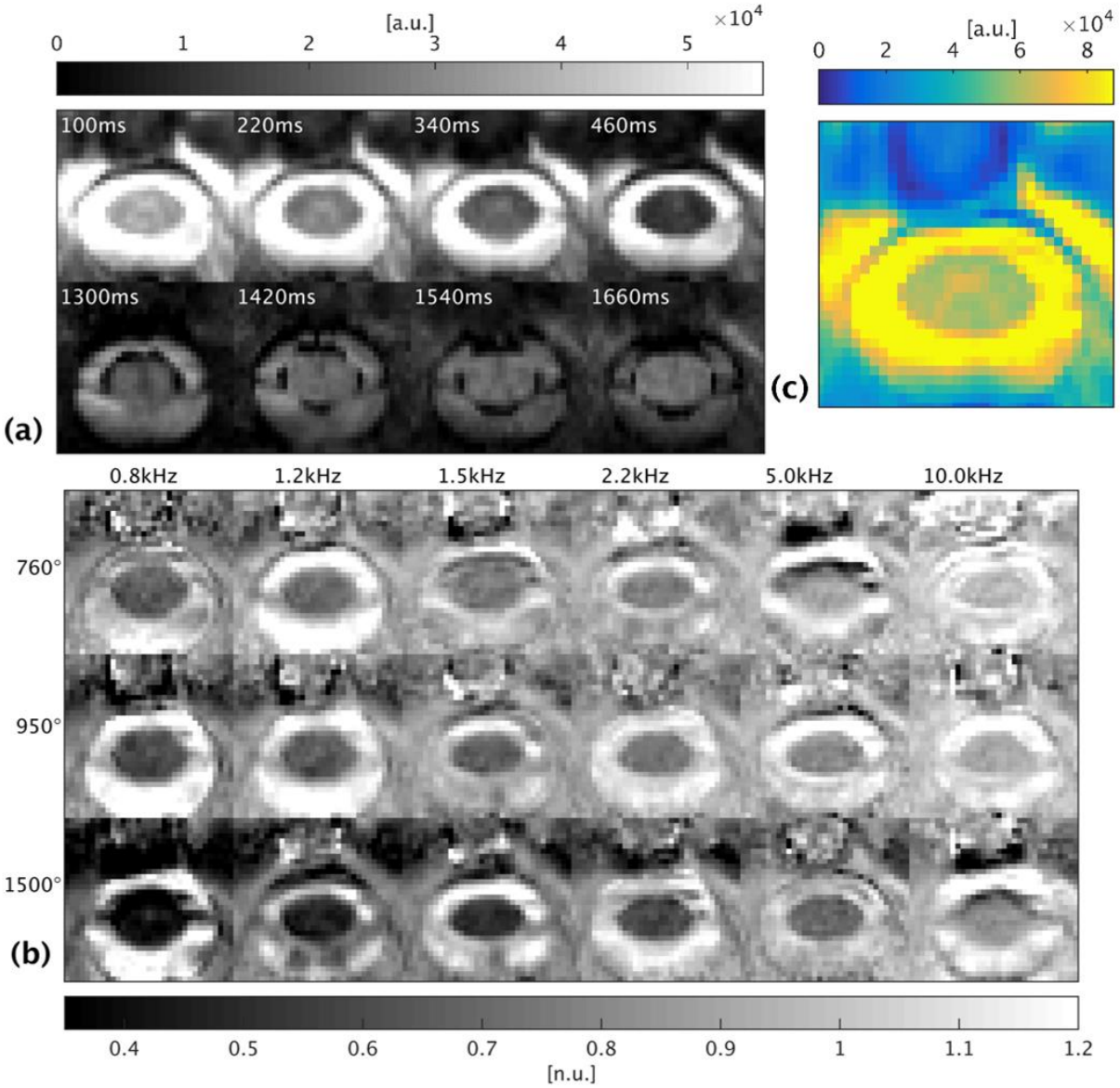


Figure 2. **(a)** IR images for different TIs. **(b)** MT-weighted images for the 18 combinations of (θ, Δ) acquired. **(c)** Reference image for motion correction and MT-weighted data intensity normalization. The same slice is shown in (a), (b) and (c).

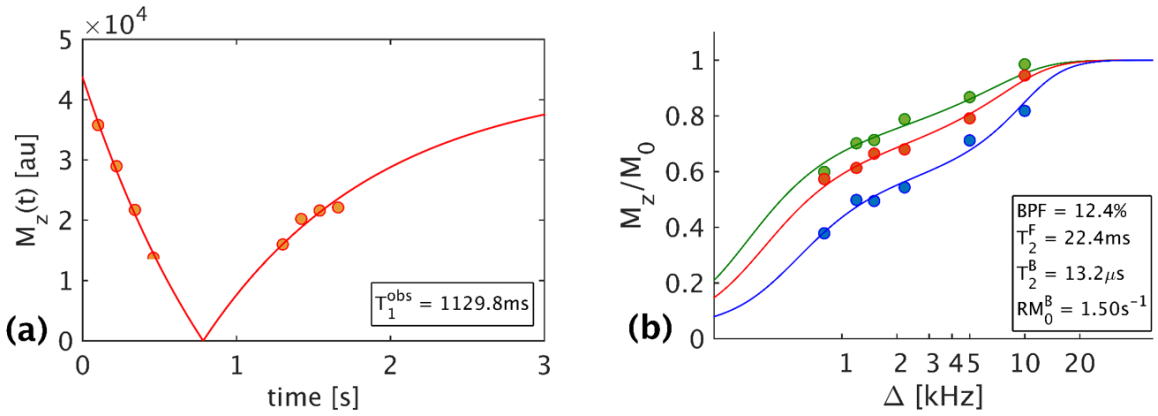


Figure 2. IR data **(a)** and MT-weighted data **(b)** fitted using their respective models in a single voxel. In (b), different colors are used to plot data and model prediction relative to different MT pulses flip angles. Optimal parameters values are reported in the boxes.

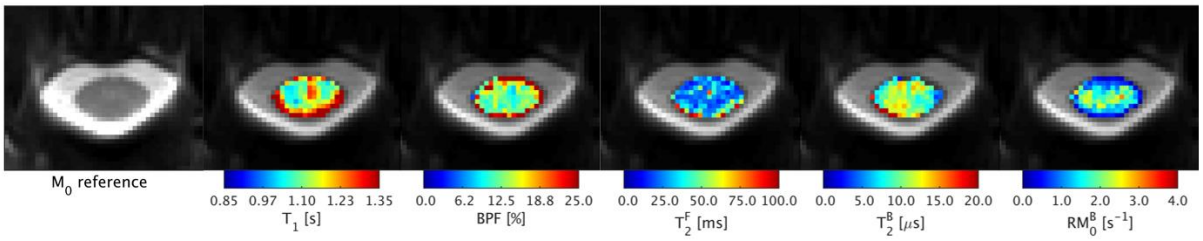


Figure 3. Parametric maps obtained from qMT model fitting, together with observed longitudinal relaxation time ($T_1^{obs}$) from IR data and $M_0$ reference image, for a single slice.

| | BPF [%] | $T_2^F$ [ms] | $T_2^B$ [$\mu$s] | $RM_0^B$ [$s^{-1}$] | $T_1^{obs}$ [ms] |
|---|---|---|---|---|---|
| 1 | 10.7 (8.1–13.9) | 44.0 (29.3–77.7) | 9.9 (7.7–12.8) | 1.74 (1.19–2.44) | 1136 (1073–1228) |
| 2 | 10.6 (8.2–14.1) | 47.0 (27.3–103.5) | 10.4 (8.6–12.3) | 1.81 (1.16–2.67) | 1091 (1038–1161) |
| 3 | 10.4 (8.1–13.9) | 51.5 (32.7–94.9) | 9.9 (7.7–12.3) | 1.63 (1.18–2.24) | 1163 (1099–1230) |

Figure 4. Whole cord median values and interquartile ranges of estimated parameters for 3 healthy volunteers.